Journal of Marine Science and Technology, Vol. 28, No. 6, pp. 622-630 (2020)
DOI: 10.6119/JMST.202012_28(6).0017

IDENTIFYING HIGH-COLLISION POTENTIAL VESSEL-BRIDGE PAIRS IN VESSEL TRAFFIC SERVICE

Jeong-Bin Yim[1] and Chun-Ki Lee[2]

Key words: vessel traffic service, vessel–bridge collision, automatic identification system, risk ratio.

ABSTRACT

Collision risk assessment for maritime traffic monitoring in vessel traffic service (VTS) is a key technology for ensuring the safety of both vessels and bridges. This study proposes a risk assessment methodology using a single measure of collision risk ratio that could assist in reducing the cognitive load of VTS operators. To explain the proposed method, we first define the semantic and mathematical relationship of vessel–bridge pier collisions; then, we establish the risk assessment framework using the collision risk ratio by combining deviation angle and stopping distance probabilities. To validate the proposed method, we conducted an experiment in the coastal waters near the Mokpo Bridge, Republic of Korea. First, we obtained automatic identification system data from the vessels; then, we assessed the vessel–bridge pier collision risk. The results confirmed the method's effectiveness in identifying high-collision potential vessel-pier pairs, allowing the determination of vessels and piers that require intensive traffic monitoring to prevent vessel–bridge collisions.

I. INTRODUCTION

Traffic safety between vessels and bridges is secured through vessel traffic service (VTS) monitoring, based on automatic identification system (AIS) data. An AIS for vessel identification and tracking was introduced by the Safety of Life at Sea amendment (IMO, 2020a). In addition, the VTS is designed to improve vessel safety and efficiency and protect the environment, as recommended by the International Maritime Organization in (IMO, 2020b).

In general, VTS operators assess collision risk subjectively through a decision-making process that combines two measures, the distance to the closest point of approach (DCPA) and the time to the closest point of approach (TCPA); however, this method causes human errors by increasing the cognitive load of VTS operators (Zhen et al., 2017). This study proposes an objective risk assessment methodology using a single measure of collision risk ratio that could assist in reducing this cognitive load.

There are two approaches to using AIS data to assess collision risk between a vessel and an object, estimating the bridge failure frequency and assessing the collision risk between vessels. The first approach is based primarily on the American Association of State Highway and Transportation Officials provision for bridge design (Barker and Puckett, 1987; Larsen, 1993). Pan et al. (2018) defined an impact scenario according to the vessel-pier collision angle, and Knott and Winters (2018) calculated the bridge failure frequency, both by using AIS data. The second approach uses two principal parameters, DCPA and TCPA. Nguyen et al. (2018) proposed a vessel collision risk estimation method using these two variables derived from AIS data, and Zhen et al. (2017) developed an AIS data analysis method to obtain a single collision risk index using a combination of DCPA and TCPA to reduce navigator cognitive load. These two approaches are concerned primarily with only bridges or vessels, respectively, which limit their direct application to vessel-pier collision risk assessment.

Consequently, we propose a collision risk assessment framework through the assessment of probabilistic vessel-pier collision risks by defining the positional relationship between vessels and bridge piers. The principal contribution of this paper is an AIS data analysis method for the identification of high-collision potential vessel-pier pairs. It consists of an acquisition process of AIS data on monitored vessels in the survey area and a risk quantification method to estimate the collision risk ratio. The risk quantification method combines two probabilities, that of the deviation angle with respect to the vessel course and that of the stopping distance (the distance at which the vessel cannot stop in front of the pier) with respect to the vessel-pier distance.

Paper submitted 06/01/20; revised 12/01/20; accepted 12/17/20. Corresponding Author: Chun-Ki Lee (e-mail: leeck@kmou.ac.kr)
[1] Division of Navigation Science, Korea Maritime and Ocean University, 727 Taejong-ro, Yeongdo-Gu, Busan, Republic of Korea
[2] Division of Navigation Science, Korea Maritime and Ocean University, 727 Taejong-ro, Yeongdo-Gu, Busan, Republic of Korea

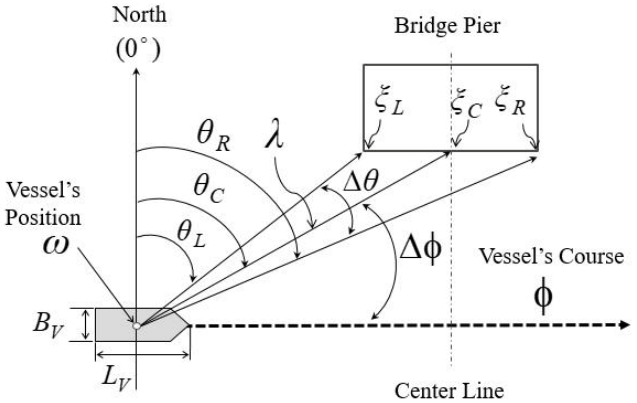

Fig. 1. Methodology to assess vessel-pier collision risk.

The proposed method was validated through scenario-based numerical simulation and then verified through experiments in the waters near Mokpo Bridge in Republic of Korea. The proposed risk assessment framework provides a more reasonable and applicable collision risk assessment for vessels traveling near existing bridges in general, compared with the current collision risk assessment approaches that are primarily concerned with bridges or vessels only. It can be used for collision risk prioritization to determine which vessels and piers require intensive traffic monitoring to prevent future collisions.

II. RISK ASSESSMENT FRAMEWORK

1. Methodology

The vessel-pier collision risk was assessed based on the collision probability arising from the positional relationship between vessels and bridge piers. Fig. 1 illustrates the methodology, showing the deviation angle $\Delta\phi$ of the vessel's course ϕ and the vessel-pier distance λ between the vessel and the pier when the vessel is traveling near the pier. This procedure assumes that the vessel-pier collision probability increases as the vessel-pier distance decreases and/or the deviation angle decreases; the validity of this assumption was confirmed in (Nguyen et al., 2018; Yim et al., 2019) for the assessment of vessel collisions. The terms and symbols shown in Fig. 1 can be explained as follows.

The vessel's position ω (latitude, longitude) is defined as its Global Positioning System (GPS) position, its length L_V as its length overall (LOA) from head to tail, and its breadth B_V as the distance between the port and the starboard center.

The bridge pier positions are defined in terms of three reference positions (ζ_L, ζ_C, and ζ_R) representing the outermost three edges of the protection file, a protruding structure that protects the bridge from vessel collisions.

The three angles (θ_L, θ_C, and θ_R) are defined to be the vessel-pier bearings, which are measured in the direction of the straight line connecting the vessel position ω and the three pier positions (ζ_L, ζ_C, and ζ_R). In addition, the angle differences $\Delta\theta$ are defined as the difference ($\Delta\theta = \theta_L \sim \theta_R$) between the angle θ_L and the angle θ_R. The deviation angles $\Delta\phi$ are defined to be the angle difference ($\Delta\phi = \phi \sim \theta_C$) between the vessel course ϕ and the angle θ_C. These vessel courses ϕ and three angles (θ_L, θ_C, and θ_R) were measured using a 360° system that measures the direction between the objects clockwise from 0° (north) to 359.9°.

The vessel-pier distances λ are defined to be the distance between the vessel position ω and the pier center position ζ_C. Moreover, to distinguish whether the vessel passed the center line of the pier, λ was considered as being of two types: if $\Delta\phi \le 90°$ then $\lambda = -\lambda$, and if $\Delta\phi > 90°$ then $\lambda = \lambda$.

We now explain the two probabilities, the deviation angle probability *PD* and the stopping distance probability *PS*, using the variables defined above.

The method for computing *PD* is based on a normal distribution curve with mean μ_θ and standard deviation (SD) σ_θ of deviation angles $\Delta\phi$, which unfortunately are difficult to obtain as a result of the low frequency of vessel-pier collisions (Kunz, 1998; Prucz and Knott, 2000; Wang and Wang, 2014). In this study, a μ_θ of 0° and a σ_θ of $\Delta\theta$ were used for this computation, as referred to in (Knott and Winters, 2018). The *PD* can be computed as the difference between θ_1 and θ_2 in the normal distribution function $F_\theta(\theta)$ and can be calculated as follows:

$$PD = |F_\theta(\theta_1) - F_\theta(\theta_2)| \tag{1}$$

$$F_\theta(\theta) = \frac{1}{\sigma_\theta\sqrt{2\pi}} \int_{-\infty}^{\theta} \exp\left[\frac{(\theta-\mu_\theta)^2}{2\sigma_\theta^2}\right] \tag{2}$$

where $\theta_1 = \Delta\varphi - \Delta\theta$ and $\theta_2 = \Delta\varphi + \Delta\theta$.

In addition to the deviation angle, vessel-pier collisions can be caused by events characterized by $\lambda \le (L_V/2)$. The collision probability according to the relationship between the vessel-pier distance λ and vessel length L_V can be derived from the stopping distance; this distance can be explained by the fact that the vessel travels a particular distance after the engine stops, as a result of inertia (IMO, 2002).

The method for computing *PS* is based on a normal distribution curve with a mean μ_λ and SD σ_λ of stopping distances; unfortunately, these are difficult to obtain as a result of the low frequency of vessel-pier collisions (Kunz, 1998; Prucz and Knott, 2000; Wang and Wang, 2014). In this study, the stopping distance was determined by the length of the vessel domain area proposed in the ship domain theory, defined as at least three times the vessel length required to prevent colliding with objects in the harbor (Goodwin, 1975; Davis et al., 1980; Fujii et al., 1984; Hansen et al., 2013). The introduction of

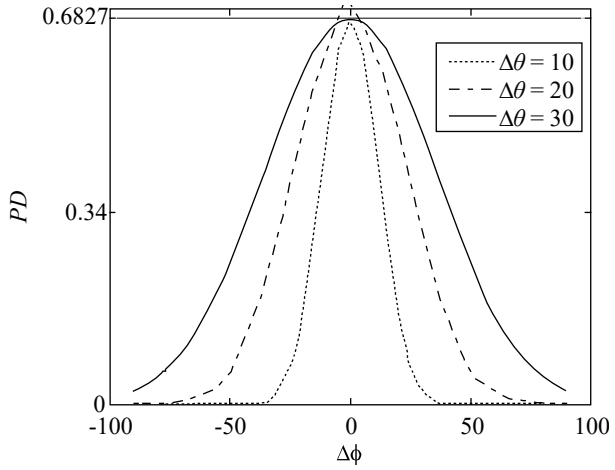

Fig. 2. Examples of the deviation angle probability $_{PD}$: deviation angle $\Delta\varphi$ vs. angle differences $\Delta\theta$ for 10°, 20° and 30.

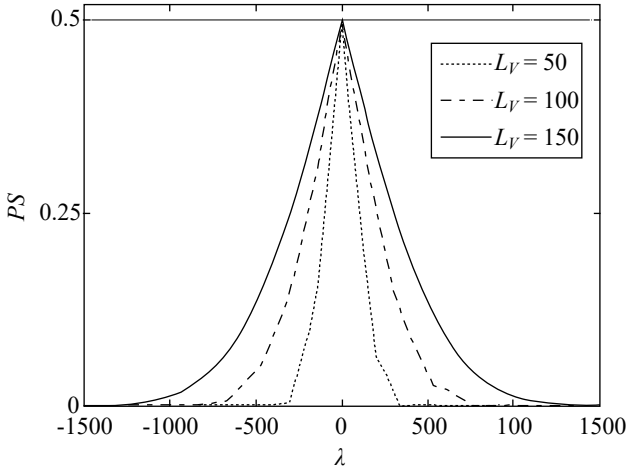

Fig. 3. Examples of the stopping distance probability PS: vessel-pier distances λ vs. vessel lengths L_V for 50, 100 and 150 *m*.

these ship domain areas resulted in $\mu_\lambda = (L_V/2)$ and, $\sigma_\lambda = \mathrm{LOA} \times 3$. The PS can be obtained from $F_\lambda(\lambda)$, where F_λ is the normal distribution function for μ_λ and σ_λ, and can be calculated as follows:

$$PS = \begin{cases} 1 - F_\lambda(\lambda); \Delta\varphi > 90^\circ \\ F_\lambda(\lambda); \quad \Delta\varphi \le 90^\circ \end{cases} \tag{3}$$

$$F_\lambda(\lambda) = \frac{1}{\sigma_\lambda\sqrt{2\pi}} \int_{-\infty}^{\lambda} \exp\left[\frac{(\lambda - \mu_\lambda)^2}{2\sigma_\lambda^2}\right] \tag{4}$$

As described previously, vessel-pier collisions can be assessed in terms of the combination of the probability *PD* for deviation angle and the probability *PS* for stopping distance. However, since these two probabilities relate to estimating the

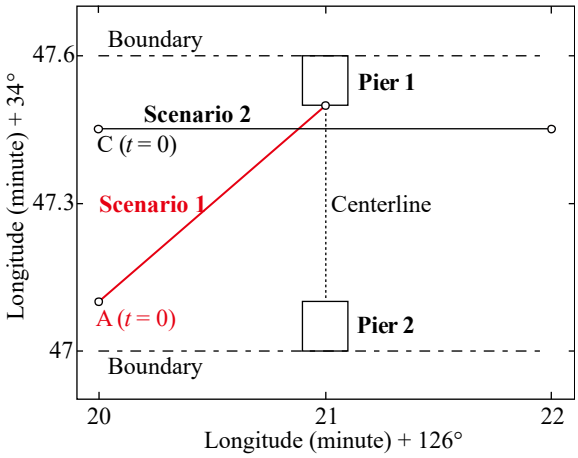

Fig. 4. Two scenarios for the validation of the method proposed in this study: Scenario 1, the vessel-pier 1 collision situation; Scenario 2, the vessel-pier 1 near miss.

expected value for the assumed event, it is difficult to apply the collision risk assessment between the vessel and the pier directly.

To solve this problem, we use the risk ratio of probability to maximum probability to assess collision risk. The vessel-pier collision risk ratio $CRR(0 \le CRR \le 1)$can be expressed as follows:

$$CRR = \left(\frac{PD}{max\,PD}\right)\left(\frac{PS}{max\,PS}\right) \tag{5}$$

where *maxPD* is the maximum probability value of *PD* calculated from (1), and *max PS* is the maximum probability value of *PS* calculated from (3). These probability values are illustrated in Figs. 2 and 3. Fig. 2 shows an example of the deviation angle probability *PD*, calculated for a deviation angle $\Delta\phi$ $(-90^\circ \le \Delta\varphi \le 90^\circ)$ vs. angle differences $\Delta\theta$ of 10°, 20°, and 30°. Moreover, Fig. 3 shows an example of the stopping distance probability *PS*, calculated for vessel-pienr distances λ $(-1500\ m \le \lambda \le 1500\ m)$ vs. vessel lengths L_V of 50 *m*, 100 *m*, and 150 *m*.

2. Validation of Risk Quantification Method

We performed a numerical simulation with two scenarios to validate the proposed risk quantification method. Both scenarios are illustrated in Fig. 4. Scenario 1 (red line) shows a collision situation in which the vessel moves from point A at time $t = 0$ to point B and collides with Pier 1. Scenario 2 (black line) shows a near miss between the vessel and Pier 1 in which the vessel moves from point C at time $t = 0$ to point D.

The collision risk ratios for both scenarios are illustrated in Fig. 5. Boxes (a) and (b) show the collision risk ratios at time t for scenario 1, and boxes (c) and (d) show the collision risk ratios for scenario 2 at time *t*. In scenario 1, the CRR_{P1} for Pier 1 increases exponentially as the vessel moves between points A to B and then reaches the maximum risk value of 1.0 (dotted

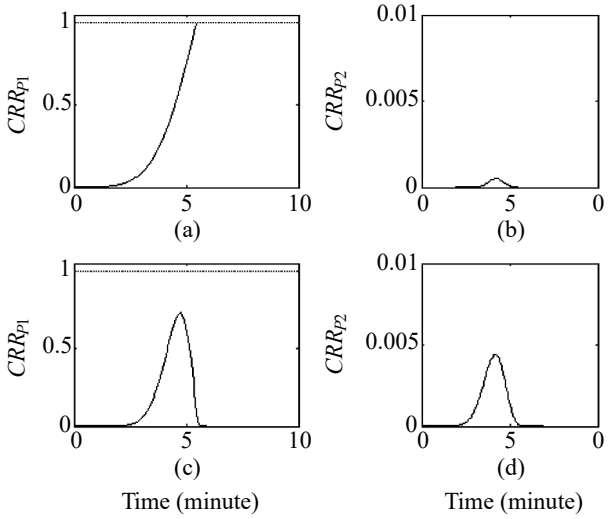

Fig. 5. Collision risk ratios (a) CRR_{P1} for Pier 1 and (b) CRR_{P2} for Pier 2 in scenario 1 (vessel-pier collision), and collision risk ratios (c) CRR_{P1} and (d) CRR_{P2} in scenario 2 (near miss).

red line). The CRR_{P2} for Pier 2 appears significantly smaller than CRR_{P1}. In scenario 2, the CRR_{P1} value increases exponentially as the vessel moves from point A to the centerline between two piers, then rapidly decreases thereafter. The CRR_{P2} tends to be similar to CRR_{P1}, but its value is small.

As a result of the above, it was confirmed that the vessel-pier collision risk can be evaluated in terms of the risk ratio using two variables (vessel-pier distance λ and deviation angle $\Delta\phi$).

III. EXPERIMENT

1. Experiment Environment

To verify the proposed collision risk assessment framework, we conducted experiments in the waters near Mokpo Bridge in Mokpo, Republic of Korea. The geographical features of the waters near Mokpo Bridge are depicted in Fig. 6, with an insert showing the survey area and AIS receiving station (Rx).

Mokpo Bridge is characterized by a 500 *m* distance between two piers and a 53 *m* clearance from sea level to the girder. Mokpo Bridge has two principal piers; the three reference positions ξ of these piers are shown in Table 1.

The water boundaries surveyed were as follows: lower left position = 34°46.40'N, 126°20.30'E; lower right position = 34°46.40'N, 126°22.00'E; upper right position = 34°47.70'N, 126°22.00'E; and upper left position = 34°47.70'N, 126°20.30'E. The water boundaries included navigable waters within a 1,852 *m* radius from the bridge center, where a high potential for vessel-pier collisions has been reported (Yim, 2010).

The Mokpo Pilot Association's recommended course ranges for inbound vessels (IBVs) and outbound vessels (OBVs) were 10°–140° and 190°–320°, respectively (Port of Mokpo,

Table 1. Three reference positions ξ (latitude + 34°N, longitude + 126°E) in minutes for Piers 1 and 2.

Class	Left ξ_L	Center ξ_C	Right ξ_R
Pier 1	(47.4650, 21.3597)	(47.4602, 21.3790)	(47.4553, 21.3983)
Pier 2	(47.2196, 21.2947)	(47.2156, 21.3138)	(47.2116, 21.3329)

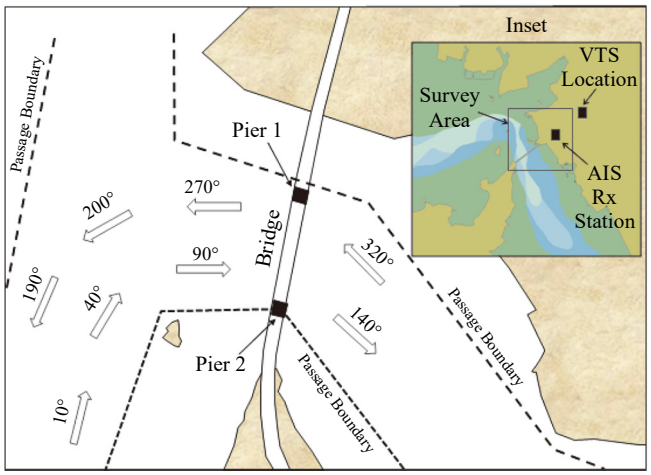

Fig. 6. Experimental environment including the boundary of the waterways surveyed, the locations of Mokpo Bridge and piers, and the recommended course (in degrees) for the safe travel of IBVs and OBVs (arrows pointing right and left, respectively).

2020); the difference between these two ranges was 130° for both vessel types, which means a 130° curved passage. According to the AASHTO provision (Baker and Puckett, 1987; Larsen, 1993), bridges crossing a passage curved by more than 45° present vessel–bridge collision risks 1.4 times greater than bridges over a straight passage.

As a result of these circumstances, the waters near Mokpo Bridge have a high vessel-pier collision potential, requiring intensive monitoring of the VTS operator. In particular, identification of high-collision potential vessel-pier pairs is necessary to assist in such monitoring.

2. AIS Data Collection and Processing

AIS data was collected using Smart Radio Holdings Limited's SR162 model, a dual-channel receiver that can receive both AIS Class A and B vessel data (Milltech Marine, 2020). AIS signals were acquired for a total of 168 h (7 days) and were stored in an Oracle structured query language data server.

The collected AIS information was converted into a data structure suitable for probability calculations. Table 2 summarizes the seven parameters derived from the collected data. The Maritime Mobile Service Identity (MMSI) number, assigned by the IMO, is used for vessel identification, along with the vessel name (up to 20 characters) as a reference. The GPS measurement time (in Korea Standard Time) is used as the

Table 2. Parameters obtained from the collected automatic identification system data.

Parameters	Description
MMSI	Maritime mobile service identity (MMSI) number
Vessel Name	Maximum 20 characters
Time	Korea Standard Time transformed from Coordinated Universal Time + 9 hours
Latitude	GPS latitude in 1/10,000 minute
Longitude	GPS longitude in 1/10,000 minute
Vessel Course	Course over ground in 1/10 degree
Reference Point	A: Distance in meters from the GPS antenna position to the vessel's head B: Distance in meters from the GPS antenna position to the vessel's stern C: Distance in meters from the GPS antenna position to the port side end D: Distance in meters from the GPS antenna position to starboard side end

Table 3. Statistics for the collected vessel data from IBVs and OBVs.

Class	Sample number	Vessel number by length range (*m*)			
		<50	50–100	100>	Sum
IBV	17636	84	30	12	126
OBV	17824	91	40	13	144
Sum	35460	175	70	25	270

time value. The four GPS antenna reference values (A, B, C, and D, in meters) are used to calculate the vessel length L_V (L_V = A+B) and breadth B_V (B_V = C+D) (both in meters).

The course over ground is used as the vessel course ϕ for the probability calculation. The GPS latitude and longitude of the vessel position ω allow the calculation of the three angles (θ_L, θ_C, and θ_R) and vessel-pier distance λ between the vessel and the piers in accordance with (6) and (7):

$$\theta = \left[\arctan\left(\frac{Med}{dLong}\right)\times\right]\left(\frac{180}{\pi}\right) \tag{6}$$

$$\lambda = \left(\frac{dLat}{\cos\theta}\right)\times 1852 \tag{7}$$

where Mea is the meridian difference calculated in accordance with (8), to which the Mercator method (Bowditch, 2019) is applied. Moreover, the longitude and latitude differences (in minutes) between the vessel and the pier ($dLong$ and $dLat$, respectively) were calculated in accordance with (9):

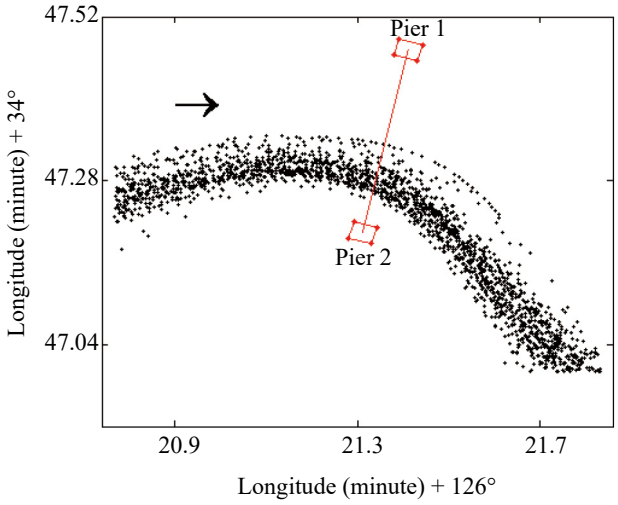

Fig. 7. Trajectories of the IBVs (represented by →) in the survey area.

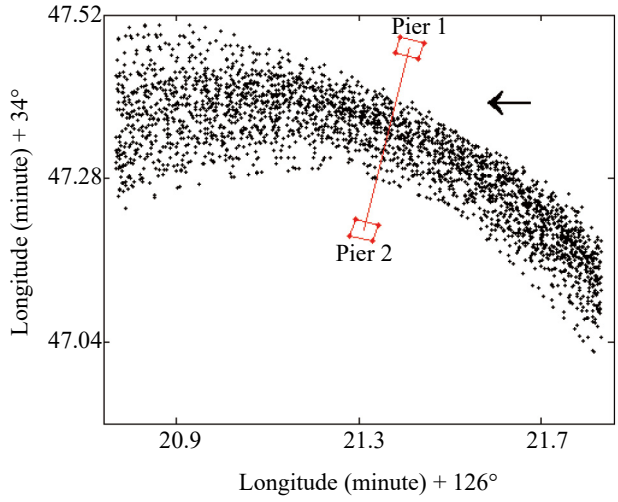

Fig. 8. Trajectories of the OBVs (represented by ←) in the survey area.

$$Med = 7915.7\times \log\left[\text{logtan}\left(\frac{\pi}{4}+\frac{Lat_C}{2}\right)-\text{logtan}\left(\frac{\pi}{4}+\frac{Lat_V}{2}\right)\right] \tag{8}$$

$$\left.\begin{aligned} dLong &= Long_V - Long_C \\ dLat &= Lat_V - lat_C \end{aligned}\right\} \tag{9}$$

where Lat_C and $Long_C$ are the latitude and longitude of the center positions ξ_C of the piers, respectively (measured directly in the field by a GPS receiver), and Lat_V and $Long_V$ are the latitude and longitude of the vessel position ω, respectively.

3. AIS Data Acquisition Results

The statistics of vessel data collected through AIS data processing are shown in Table 3. The numbers of IBV and OBV

Table 4. One-way ANOVA results of the collision risk ratios for IBVs.

Source	SS	Df	MS	*F*	*p*-Value
Ratios	0.0011	1	0.0011	15.15	<0.001*
Error	0.3048	4032	7.56×10^{-5}		
Total	0.3059	4033			

SS, sum of squares; Df, degrees of freedom; MS, mean squares; *F*, *F* statistics.
* *P*<0.01.

Table 5. One-way ANOVA results of the collision risk ratios for OBVs.

Source	SS	Df	MS	*F*	*p*-Value
Ratios	0.0043	1	0.0043	46.95	<0.001*
Error	0.4829	5270	9.16×10^{-5}		
Total	0.3059	4033			

SS, sum of squares; Df, degrees of freedom; MS, mean squares; *F*, *F* statistics.
* *P*<0.01.

Table 6. Mean and SD of the collision risk ratios ($\times10^2$) for a vessel-pier pair.

Class	CRR_{P1}		CRR_{P2}	
	Mean	SD	Mean	SD
IBV	0.0456	0.8541	0.1522	0.8844
OBV	0.1829	1.3532	0.0022	0.0397

IBV, inbound vessel; OBV, outbound vessel; CRR_{P1}, collision risk ratio for Pier 1; CRR_{P2}, collision risk ratio for Pier 2.

data samples (17,636 and 17,824, respectively) were counted equally over 1,000 units. The total number of transit vessels of different length ranges was 270 for seven days, and their minimum and maximum lengths were 39 and 199 *m*, respectively. This diversity implies that the data are suitable for evaluating the vessel-pier collision risk.

Figs. 7 and 8 show the trajectories of the IBVs and OBVs, respectively. The IBV trajectories are closer to Pier 2, while the OBV trajectories converge slightly toward Pier 1. The corresponding statistical results revealed that the IBV-Pier 2 distance (mean = 156.21, SD = 41.24) was 55.88 *m* shorter than the OBV-Pier 1 distance (mean = 212.09, SD = 52.38).

IV. RISK ASSESSMENT RESULTS

1. ANOVA of Collision Risk Ratios

A one-way analysis of variance (ANOVA) was performed to test the significance of the collision risk ratio pairs calculated between the two piers and the vessels.

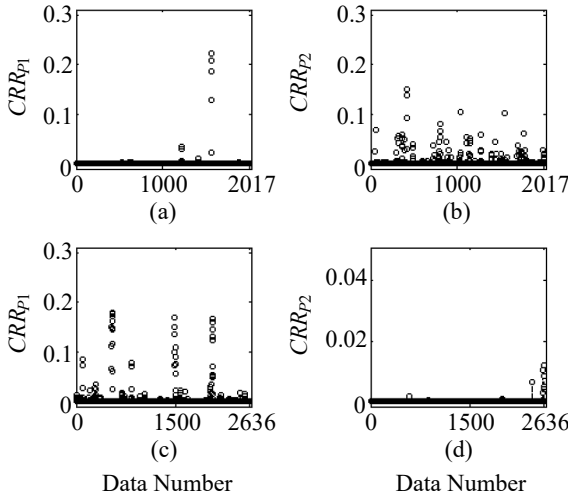

Fig. 9. Collision risk ratios of the (a, b) IBVs and (c, d) OBVs for (a, c) Pier 1 and (b, d) Pier 2.

The calculation results are illustrated in Fig. 9; the boxes (a) and (b) represent CRR_{P1} and CRR_{P2} for IBVs of data length 2,017, and the boxes (c) and (d) represent CRR_{P1} and CRR_{P2} for OBVs of data length 2,636. Overall, IBVs show larger CRR_{P2} than CRR_{P1}, while OBVs show larger CRR_{P1} than CRR_{P2}.

Tables 4 and 5 show ANOVA results for the group $\{CRR_{P1}, CRR_{P2}\}$ of collision risk ratios for IBVs and OBVs, respectively. The significant differences, [$F(1, 4033) = 15.15$, $p < 0.01$] for IBVs and [$F(1, 4033) = 46.95$, $p < 0.01$] for OBVs, were observed. This confirmed that the two collision risk ratios for IBVs and OBVs were significantly different at the 99% confidence level ($p = 0.01$). Thus, the two collision risk ratios allow the collision risk comparison of vessel-pier pairs.

2. Comparison of Vessel-Pier Collision Risk

To identify which vessel-pier pairs have a high-collision risk, the average values of the collision risk ratios were compared. In addition, two comparisons were performed; between daytime and nighttime and between small and large vessels.

Table 6 shows the mean and standard deviation (SD) of collision risk ratios ($\times10^2$) for IBVs and OBVs, and the analysis results can be summarized as follows. For IBVs and OBVs, the IBV–CRR_{P2} (mean = 0.1522, SD = 0.8844) is 3.34 times as large as the corresponding IBV–CRR_{P1} (mean = 0.0456, SD = 0.8541), while an OBV–CRR_{P1} (mean = 0.1829, SD = 1.3532) is 83.14 times as large as the corresponding OBV–CRR_{P2} (mean = 0.0022, SD = 0.0397). In addition, for each CRR_{P1} and CRR_{P2}, the OBV–CRR_{P1} (mean = 0.1829) is 4.01 times as large as the corresponding IBV–CRR_{P1} (mean = 0.0456), while the IBV–CRR_{P2} (mean = 0.1522) is 69.18

Table 7. Mean and SD of the collision risk ratio ($\times 10^2$) of vessel-pier pairs classified into daytime and nighttime.

Class	Time zone	CRR_{P1}		CRR_{P2}	
		Mean	SD	Mean	SD
IBV	Daytime	0.0619	1.0007	0.1432	0.8669
	Nighttime	0.0019	0.0205	0.1762	0.9301
OBV	Daytime	0.2184	1.5114	0.0027	0.0444
	Nighttime	0.0445	0.2133	$< 10^{-5}$	0.0004

IBV, inbound vessel; OBV, outbound vessel; CRR_{P1}, collision risk ratio for Pier 1; CRR_{P2}, collision risk ratio for Pier 2; Daytime, 6:00 AM–6:00 PM; Nighttime, 6:00 PM–6:00 AM.

Table 8. Mean and SD of the collision risk ratio ($\times 10^2$) of vessel-pier pairs classified into small and large vessels.

Class	Vessel size	CRR_{P1}		CRR_{P2}	
		Mean	SD	Mean	SD
IBV	Small	$< 10^{-5}$	$< 10^{-5}$	0.1391	0.9089
	Large	0.1476	1.5328	0.1814	0.8269
OBV	Small	0.0094	0.0955	$< 10^{-5}$	0.0001
	Large	0.4339	2.0891	0.0053	0.0619

times as large as the corresponding OBV–CRR_{P2} (mean = 0.0022). Finally, for the vessel-pier pair, the OBV–CRR_{P1} (mean = 0.1829) is 1.2 times as large as the corresponding IBV–CRR_{P2} (mean = 0.1522).

Table 7 shows the mean and SD of the collision risk ratio ($\times 10^2$) for the vessel-pier pair, which is classified into daytime, 6:00 AM–6:00 PM, and nighttime 6:00 PM–6:00 AM. As a result, during the daytime, the IBV–CRR_{P1} (0.0619) is larger, but, during the nighttime, the OBV–CRR_{P2} (0.1762) is larger. Moreover, during the nighttime, the IBV–CRR_{P2} (0.1762) is 92.73 times as large as IBV–CRR_{P1} (0.0019), and during the daytime, the OBV–CRR_{P1} (0.2184) is 80.89 times as large as OBV–CRR_{P2} (0.0027).

Table 8 shows the mean and SD of the collision risk ratio ($\times 10^2$) for the vessel-pier pair, classified into small vessels ($\mathrm{LOA} < 50m$) and large vessels ($\mathrm{LOA} \geq 50m$). As a result, all large vessels have a higher collision risk ratio than all small vessels. Moreover, on IBV's large vessel, the IBV–CRR_{P2} (0.1814) is 1.23 times as large as the corresponding IBV–CRR_{P1} (0.1476), but, on OBV's large vessel, the OBV–CRR_{P1} (0.4339) is 81.87 times as large as the corresponding OBV–CRR_{P2} (0.0053).

We summarize these three analysis results as follows: for the IBVs, large vessels ($\mathrm{LOA} \geq 50m$) have a greater risk of collision with Pier 2 during nighttime, whereas, for the OBVs, large vessels have a greater risk of collision with Pier 1 during daytime.

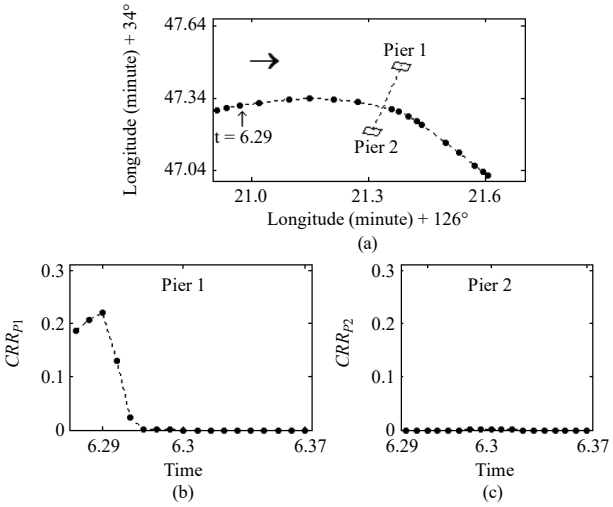

Fig. 10. Trajectory and collision risk ratios of the IBV (MMSI 354183000): (a) the trajectory of the vessel, (b) the collision risk ratio for Pier 1, and (c) the collision risk ratio for Pier 2.

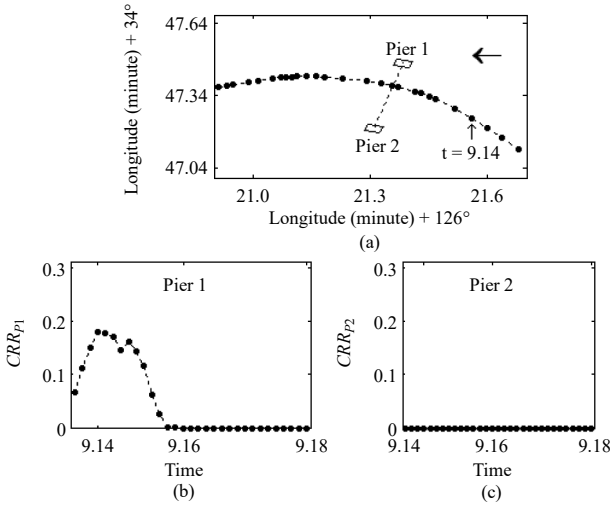

Fig. 11 Trajectory and collision risk ratio of the OBV (MMSI 44012238): (a) the trajectory of the vessel, (b) the collision risk ratio for Pier 1, and (c) the collision risk ratio for pier 2.

This can be considered as confirming that the proposed risk assessment method can be successfully applied to determine which ship type has a large collision potential at which pier and in which time intervals.

3. Visual Collision Risk Analysis Over Time

We performed a visual collision risk analysis over time to verify the applicability of the proposed risk assessment method to vessel-pier collision risk monitoring. Vessels with the highest-collision risk ratios among IBVs and OBVs shown in Table 9 were examined; the trajectory and collision risk ratios over time for these vessels are illustrated in Figs. 10 and 11.

Table 9 shows a summary of the identification results for both the IBV and OBV, including ship specification (IMO

Table 9. Identification results of vessel-pier pairs with the highest collision risk ratios for both an IBV and an OBV.

Class	IBV	OBV
MMI	354183000	44012238
LOA	199	144
Breath	32	25
t_{max}	6.29	9.14
λ_{P1}	−681.86	−485.32
λ_{P2}	−551.74	−376.93
CRR_{P1}	0.2215	0.1799
CRR_{P2}	$<10^{-5}$	$<10^{-5}$

IBV, inbound vessel; OBV, outbound vessel; MMSI, maritime mobile service identity; LOA, length overall; t_{max}, time (hours) when collision risk is maximum; λ_{P1}, vessel-Pier 1 distance; λ_{P2}, vessel-Pier 2 distance; CRR_{P1}, collision risk ratio for Pier 1; CRR_{P2}, collision risk ratio for Pier 2.

number, LOA, and breadth), time t_{max} of maximum collision risk, and both vessel-pier distance (λ_{P1} and λ_{P2}) and collision risk ratios (CRR_{P1} and CRR_{P2}) at t_{max}. In the IBV, the CRR_{P1} has a maximum value of 0.2215 at 6.29 hours (6:17 AM), before passing between Piers 1 and 2, because both vessel-pier distances ($\lambda_{P1} = -681.86$, $\lambda_{P2} = -551.74$) are negative. Moreover, in OBV, the CRR_{P1} has a maximum value of 0.1799 at 9.14 hours (9:08 AM), before passing between Piers 1 and 2, because both vessel-pier distances ($\lambda_{P1} = -485.32$, $\lambda_{P2} = -376.93$) are negative.

In Fig. 10(a) for the IBV, before the vessel passes between the piers, it looks closer to Pier 2, but its course appears to be heading to Pier 1. As a result, in Fig. 10(b), the value of CRR_{P1} for Pier 1 was maximized at 6.29 hours. Moreover, in Fig. 11(a) for the OBV, before the vessel passes between the piers, it looks closer to Pier 1, and its course appears to be heading to Pier 1. As a result, in Fig. 11(b), the value of CRR_{P1} for Pier 1 was maximized at 9.14 hours.

These results can be considered as confirming the validity of the collision risk ratio calculated over time for the distance and bearing between the vessel and the pier; consequently, the proposed risk assessment method can be applied as a means of monitoring vessel-pier collision risk.

V. DISCUSSION

The risk assessment framework of vessel-pier collision proposed in this study uses primarily two variables, the vessel-pier deviation angle and the vessel-pier stopping distance. However, various variables can affect vessel-pier collisions, including route characteristics, weather, traffic density, and darkness (Larsen, 1993; Kunz, 1998; Cho, 2020). We have also observed previously that navigator human errors (i.e., failures and errors in situational awareness) have a significant impact on these collisions (Yim, 2017; Yim et al., 2018; Youn et al., 2019).

Thus, more sophisticated technical improvements in the study of vessel-pier collisions are required in this regard.

VI. CONCLUSSIONS AND FUTURE WORK

The findings of this study on high-collision potential vessel-pier pair identification using a risk assessment framework can be summarized into the three following results.

First, high-collision potential vessel-pier pairs were identified using a single measure of collision risk ratio using a combination of probabilities for deviation angle and stopping distance between the vessel and pier.

Second, the collision risks between the vessel and the pier were assessed effectively through the developed risk assessment framework of vessel-pier collision.

Finally, the proposed collision risk method can provide vessel-pier collision monitoring over time based on AIS data.

Therefore, the proposed collision risk assessment framework could be applied for risk assessment of collisions between various types of vessels and piers with various geographical features. As future work, we will examine a revision of the collision risk assessment method using the collision probability proposed in this study with different types of variables that affect vessel-pier collision risk, and their effectiveness will be evaluated by comparison with the two measures DCPA and TCPA.

ACKNOWLEDGMENT

This research was supported by the 'Development of Autonomous Ship Technology(20200615, Development of Shore Remote Control System of MASS)' funded by the Ministry of Oceans and Fisheries (MOF, Korea). The authors would like to thank Enago (www.enago.co.kr) for the English language review.

REFERENCES

Barker, R. M. and J. A. Puckett (1987). Design of highway bridges based on AASHTO LRFD bridge design specifications. Wiley and Sons, New York, USA, 1–1169.

Bowditch, N. (2019). Chapter 12-The sailings. In American practical navigator: an epitome of navigation, edited by Gerard J. and Clifford, Jr., National Geospatial-Intelligence Agency: Springfield, Virginia, USA, 193–213.

Cho, D. Y. (2020). Design wind speed estimation for long span bridge in Korean southern and western coast. International Journal of Engineering and Technology Innovation, 10, 146-155.

Davis, P. V., M. J. Dove and C. T. Stockel (1980). A computer simulation of marine traffic using domains and arenas. The Journal of Navigation, 33, 215–222.

Fujii, Y., H. Yamanouchi and T. S. Matui (1984). Survey on vessel traffic management systems and brief introduction to marine traffic studies, Electronic Navigation Research Institute Papers (in Japan), 84.

Goodwin, E. M. (1975). A statistical study of ship domains. The journal of Navigation, 28, 328–344.

Hansen, M. G., T. K. Jensen, T. Lehn-Schiøler, K. Melchild, F. M. Rasmussen and F. Ennemark (2013). Empirical ship domain based on AIS data. The Journal of Navigation, 66, 931–940.

IMO (2002). Explanatory Notes to the Standards for Ship Manoeuvrability, MSC/Circ. 1053.

IMO (2020a). AIS transponders. Available online: http://www.imo.org/en/OurWork/Safety/Navigation/Pages/AIS.aspx (accessed on 20 July 2020).

IMO (2020b). Vessel traffic services. Available online: http://www.imo.org/en/OurWork/Safety/Navigation/Pages/VesselTrafficServices.aspx (accessed on 20 July 2020).

Knott, M and M. Winters (2018). Ship and barge collisions with bridges over navigable waterways. Proceeding of the 34th PIANC World Congress, Panama City, Panama, 1–16.

Kunz, C. U. (1998). Ship bridge collision in river traffic, analysis and design practice. In Ship Collision Analysis, Proceedings of the international symposium on advances in ship collision analysis, Copenhagen, Denmark, edited by Gluver, H., CRC Press, Florida, USA, 259–279.

Larsen, O. D. (1993). Ship collision with bridges: The interaction between vessel traffic and bridge structures (Vol. 4). IABSE, Zurich, Switzerland, 37–51.

Milltech Marine (2020). Smart Radio SR161/SR162/SR162G AIS Receiver Operation & Installation Manual. Available online: http://www.milltechmarine.com/customer_center/Smart_Radio_AIS_Receiver.pdf (accessed on 20 July 2020).

Nguyen, M., S. Zhang and X. Wang (2018). A novel method for risk assessment and simulation of collision avoidance for vessels based on AIS. Algorithms, 11, 204.

Pan, J., Y. Wang and M. C. Xu (2018). Impact Scenario Models of Ship-Bridge Collision Based on AIS Data. Proceeding of the 28th International Ocean and Polar Engineering Conference, Sapporo, Japan, 557–563.

Prucz, Z. and M. Knott (2000). Vessel Collision Design of Bridges. In Bridge Engineering Handbook, edited by Chen, W. F. and Duan L., CRC Press, Florida, USA, 259–279.

Port of Mokpo. Available online: http://mokpo.mof.go.kr/content/view.do (accessed on 20 July 2020).

Wang, J. and W. Wang (2014). Estimation of vessel-bridge collision probability for complex navigation channels. Journal of Bridge Engineering, 20, 04014091.

Yim, J. B. (2017). A study on the analysis and identification of seafarers' skill-rule-knowledge inherent in maritime accidents. Journal of the Korean Society of Marine Environment and Safety, 23, 224–230.

Yim, J. B., D. S. Kim and D. J. Park (2018). Modeling perceived collision risk in vessel encounter situations. Ocean Engineering, 166, 64–75.

Yim, J. B., D. J. Park and I. H. Youn (2019). Development of navigator behavior models for the evaluation of collision avoidance behavior in the collision-prone navigation environment. Applied Sciences, 9, 3114.

Yim, J. B. (2010). Development of collision risk evaluation model between passing vessel and Mokpo harbor bridge. Journal of Navigation and Port Research, 34, 405–415.

Youn, I. H., D. J. Park and J. B. Yim (2019). Analysis of lookout activity in a simulated environment to investigate maritime accidents caused by human error. Applied Sciences, 9, 4.

Zhen, R., M. Riveiro, M. and Y. Jin (2017). A novel analytic framework of real-time multi-vessel collision risk assessment for maritime traffic surveillance. Ocean Engineering, 145, 492–501.